Experimental Analysis of a Pitot-Type Air Intake

Dieter Welte*
Dornier GmbH, Friedrichshafen, Federal Republic of Germany

A pitot-type air inlet in an underbelly location was designed for a single-engine, supersonic fighter configuration. Compared to a similar inlet of an existing lightweight fighter aircraft, a fuselage-integrated 11-deg ramp in front of the inlet was chosen to extend the Mach number for good total pressure recovery up to 1.6. A wind tunnel program was performed at low and high speeds and up to very high angles of attack. The test results are discussed, and an analysis of the supersonic inlet flowfield is presented.

Nomenclature

A = area
A_0/A_{HL} = capture area ratio
a, b = length of major and minor axis of ellipse, respectively
C_D = axial force coefficient, $=D/q_0A_1$
CI = circumference of lip
C_p = pressure coefficient, $=(P-P_0)/q_0$
D = axial force of air intake
DC_{60} = distortion index; difference of worst 60-deg segment from mean total pressure divided by mean dynamic pressure at engine face
I = distortion index; maximum total pressure difference divided by mean total pressure at engine face
M = Mach number
$\dot{m}$ = mass, flow, reduced to static and standard conditions based on freestream total pressure and temperature
$\dot{m}_{max}$ = maximum mass flow for $M_0=0.7$ (choked flow in throat)
P = static pressure
P_t = total pressure
$\bar{P}_t$ = mean total pressure
q = dynamic pressure
α = angle of attack
β = angle of yaw
η = total pressure recovery, $=\bar{P}_{t2}/P_{t0}$

Subscripts

HL = highlight
1 = throat
2 = engine face
0 = freestream

Introduction

IN preparation for a future supersonic fighter program, the Ministry of Defense has, since 1978, sponsored a technology program for supersonic air inlets. The aim of the program is to extend the knowledge of design methods, test procedures, and theoretical analysis methods.

Dornier took part in this program with a pitot-type air inlet configuration. The pitot-type inlet is a promising configuration for a lightweight and low-cost fighter with the primary mission to Mach 1.6. The fabrication of the model and the wind tunnel tests were performed by Deutsche Forschungs- und Versuchsanstalt für Luft- und Raumfahrt (DFVLR).

The pitot-type air inlet in an underbelly location was chosen because this configuration is relatively simple for empirical and theoretical analysis methods and there exists a well-documented[1,2] similar configuration, the YF-16 inlet, which was a helpful guide for the EM-1 program. The YF-16 air inlet

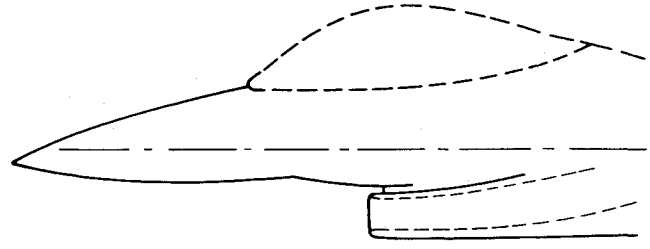

a) Pitot-type design in an underbelly location with a fuselage integrated 11-ramp and boundary layer split by the inlet lip.

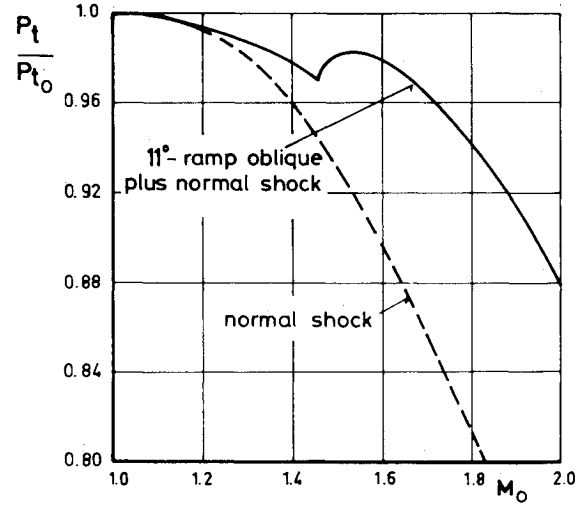

b) Calculated total pressure recovery plotted against Mach number using simple supersonic two-dimensional flow theory. The Dornier supersonic air inlet design provides better pressure recovery to higher Mach numbers than a pure pitot-type inlet.

Fig. 1 Dornier supersonic air inlet design characteristics.

Received Oct. 24, 1984; revision received Oct. 17, 1985.

*Head, Aircraft Project Aerodynamics Group.

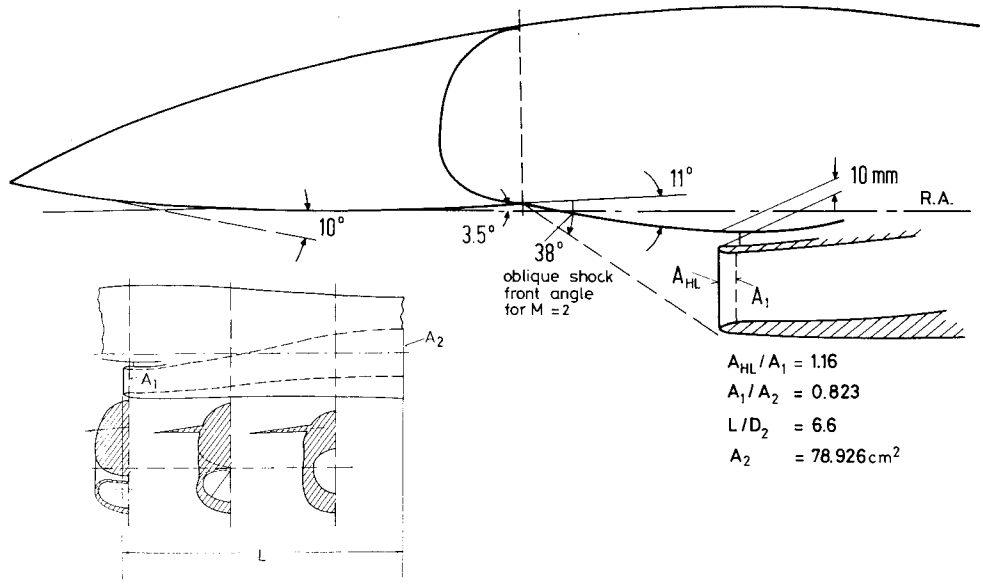

Fig. 2 EM-1 air inlet wind tunnel model, main dimensions.

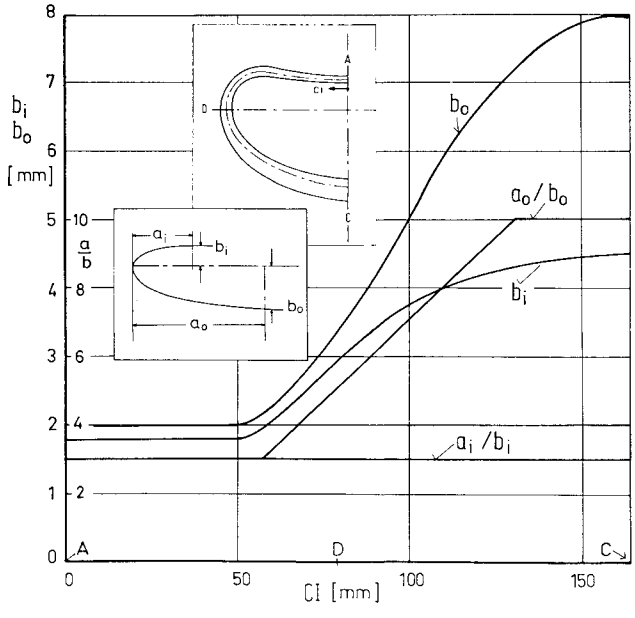

Fig. 3 EM-1 lip dimensions.

is a fixed-geometry, normal-shock inlet design. The underbelly inlet location provides fuselage shielding to enhance maneuverability, i.e., there is no degradation in pressure recovery to 30-deg angle of attack and stable operation to 40 deg subsonically, with an increase in pressure recovery with the angle of attack at supersonic speeds.

Inlet Design and Description

The Dornier supersonic EM-1 air inlet is a fixed-geometry, pitot-type inlet design with a fuselage-integrated, 11-deg ramp and boundary-layer diverter at the inlet lip and underbelly inlet location. This design was expected to perform similar to a pitot inlet and to provide good total pressure recovery to higher Mach numbers.

The EM-1 design concept is shown top of Fig. 1 and on the bottom the calculated total pressure recovery is plotted against Mach number using simple supersonic two-dimensional flow theory. The upper inlet lip is displaced from the ramp to eliminate boundary-layer ingestion. Total pressure recovery by a simple shock is 98% for $M=1.3$ and 96% for $M=1.4$ with a steep decrease for increasing Mach numbers. The same figure shows the theoretical total pressure recovery for an 11-deg ramp oblique plus normal shock. Ninety-eight percent total pressure recovery is achieved up to Mach 1.6 and 96% for M-1.7.

A side view of the inlet design and its integration into the fuselage is shown in Fig. 2. The angle between the fuselage lower surface and the reference axis is 10 deg at the nose cone. This angle decreases downstream and is −3.5-deg in front of the ramp. This number was chosen in favor of good pressure recovery for high-g maneuvers. The ramp deflection angle is 11 deg. The length of the ramp is set by the oblique shock at Mach 2 being tangent to the lower lip. The vertical distance between the ramp and the upper lip is set at 10 mm corresponding to the boundary-layer thickness. The area ratio of highlight to throat is 1.16. The duct cross section transitions from kidney-shaped to circular at the engine face. The area distribution provides a near-linear Mach number change from the throat to the compressor face to minimize diffuser losses. The area ratio of throat to engine face is 0.823. The length-to-diameter ratio of the duct is 6.6. The vertical offset of the duct centerline between the throat and the engine face is 0.072 times the duct length. The diameter of the duct at the engine face is 109 mm.

The front view of the inlet and the lofting characteristics are shown in Fig. 3. In the front view the inlet is kidney shaped, built up of one circular and two elliptical sections. The inlet cowl features a moderately blunt lower lip to avoid separation for the high angle-of-attack conditions. The upper lip is sharper since it is less prone to separation because of the shielding effect of the fuselage. The outer and inner lip sections are built up of ellipses with an axis ratio of 3, with the inner lip 10% smaller than the outer. The lower lip is 2.5 times greater than the upper lip with a smooth lofting.

Description of the Wind Tunnel Model and Test Equipment

A general view of the inlet model EM-1 is shown in Fig. 4. The model consists of the body, the inlet with duct, the unit containing the rotating pitot rake and the throttle to control the mass flow, the support sting, and finally the front part of a wing leading-edge extension. The model has no canopy since this is a basic study. In the low-speed range the inlet flow was simulated by suction with vacuum pumps that were connected to the model exit with flexible pipes.

The model length is approximately 150 cm and the body width is approximately 15 cm. The outer diameter of the duct at the engine face is 10.9 cm. The model size is approximately 12.5%-scale of a hypothetical aircraft.

More than 200 static pressure taps were installed on the forebody and ramp, around the lip (6 sections), and inside the

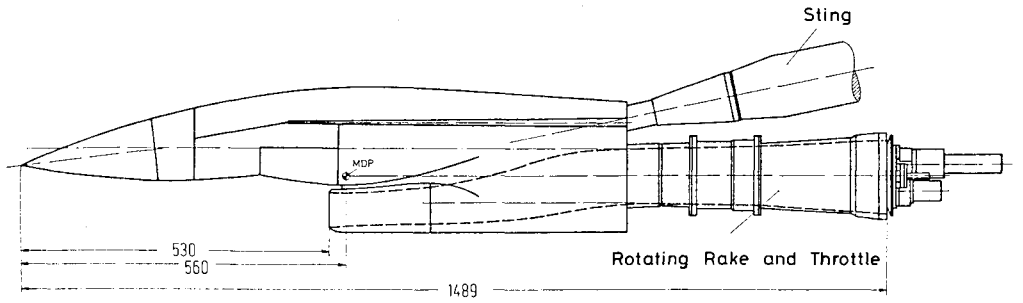

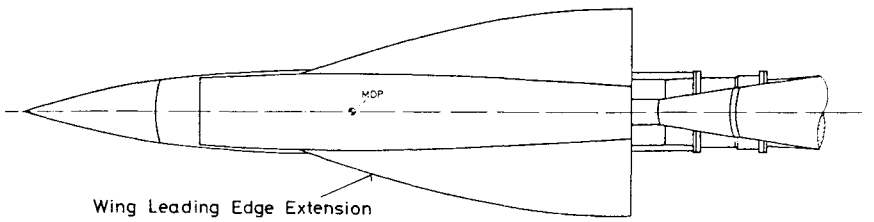

Fig. 4 General view of EM-1 model.

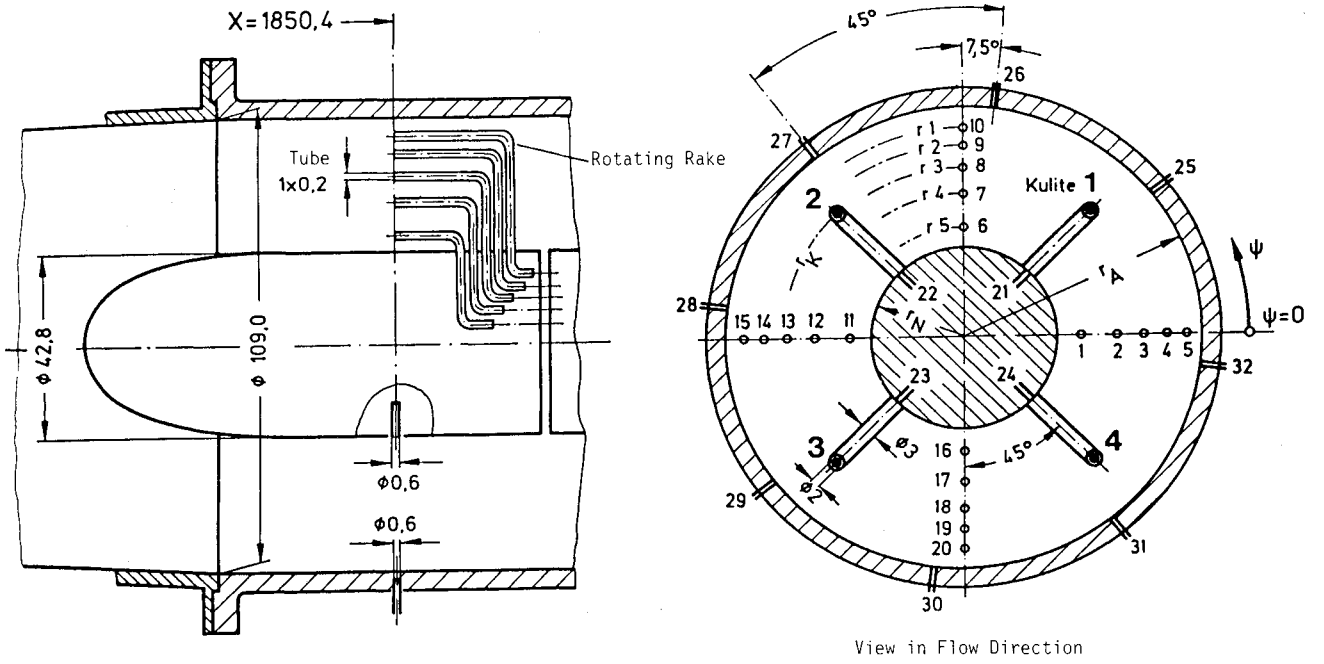

Fig. 5 Pressure probes at the engine face.

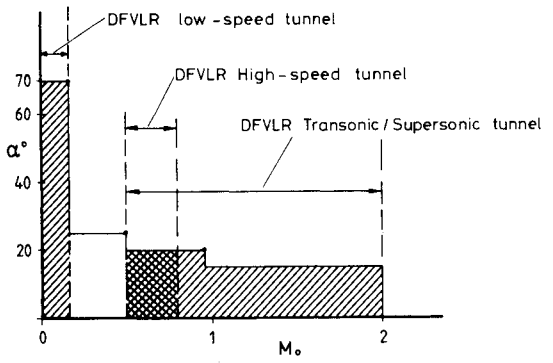

Fig. 6 Test facilities and test range for EM-1 tests.

Table 1 DFVLR wind tunnel

	Low speed	High speed	Transonic/ supersonic
Tunnel type	Closed circuit	Suckdown	Closed circuit, pressurized
Test-section type	Open or closed	Open	Closed, perforated walls
Test-section size, m^2	3.6×3.6	0.75×0.75	1×1

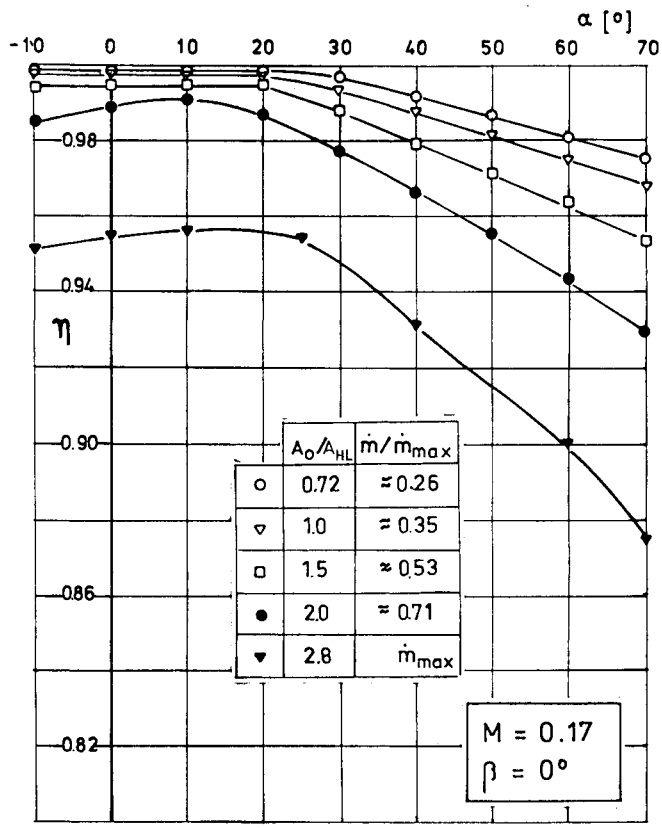

Fig. 7 Total pressure recovery; effect of capture area ratio and angle of attack.

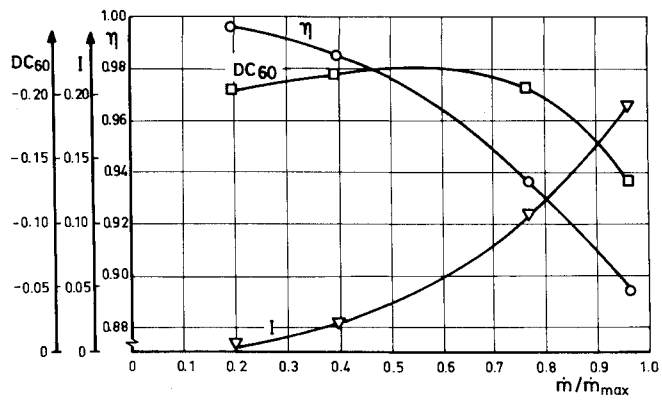

Fig. 8 Static inlet performance.

duct. At the compressor face, four radial rakes, each with five pitot tubes, were located as shown in Fig. 5. This rake assembly could be rotated in angular steps of 15 deg so that 120 total pressure readings per run were taken. The mass flow was calculated from the pressures in the engine face. The effect of the boundary layer was taken into account by a calibration factor determined in the low-speed test with a calibrated Venturi pipe.

Test Facilities and Range of the EM-1 Test

The tests were performed in the DFVLR wind tunnel facilities. Figure 6 and Table 1 summarizes the tunnel characteristics and the test range. The low-speed wind tunnel has a closed circuit. For these tests the open test section with an area of $3.6 \times 3.6\ m^2$ was used. The Mach numbers for these tests were 0.09 and 0.17, the maximum angle of attack was 70 deg, and the maximum yaw angle was 12 deg.

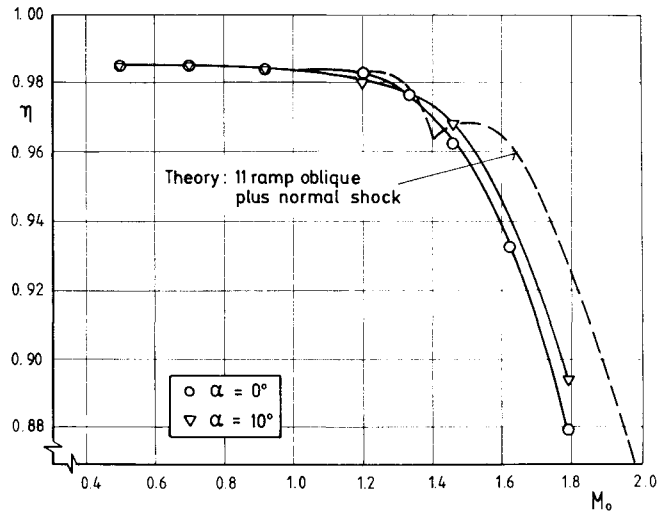

Fig. 9 Total pressure recovery vs Mach number, $M_1 = 0.75$.

Some preliminary high-speed tests in the range $0.5 \leq M \leq 0.8$ were conducted in the suck-down high-speed tunnel with an open test section of $0.75 \times 0.75\ m^2$ cross section.

Most of the high-speed tests were made in the transonic/supersonic wind tunnel, a closed-circuit, pressurized tunnel. The test section of $1 \times 1\ m^2$ cross section has perforated walls to eliminate wall interference effects. For these tests the maximum angle of attack was 20 deg for Mach numbers up to 0.95. For the Mach number range from 1.05 to 2.00, the maximum angle of attack was 15 deg. The maximum angle of yaw was 12 deg.

Pressure Recovery and Distortion at Low Speeds

The performance of the inlet at low speeds and static conditions is shown in Figs. 7 and 8. In Fig. 7 the pressure recovery is plotted against angle of attack (α) for different capture area ratios. Figure 7 shows that the pressure recovery decreases with increasing α and increasing capture area ratio. There is no linear decrease of total pressure recovery, however, a sudden break is obvious at around an angle of attack of 30 deg and a capture area ratio around 2. At these conditions the measured static pressures around the lip show flow separation inside the lip.

The influence of yaw angle (β) on the total pressure recovery is small for angles between 0 and 12 deg.

The total pressure recovery and the distortion indices I and DC_{60} for the static condition are plotted vs nondimensionalized mass flow in Fig. 8. For maximum mass flow the total pressure recovery is 90% or 10% the total pressure loss. The total pressure loss $(1-\eta)$ and the distortion index I increase from low mass flow to maximum mass flow by a factor of roughly 10, whereas the distortion parameter DC_{60} does not change by more than a factor of 1.3. The reason is that, as a rough approximation, the losses are proportional to the dynamic pressure of the flow inside the duct. This means that the total pressure loss and the distortion index I increases approximately with the second power of the mass flow, see Fig. 8. Since the distortion parameter DC_{60} includes, by definition, the dynamic pressure at the engine face in the denominator, the influence of the mass flow on DC_{60} is relatively small. The small variation of DC_{60} with the mass flow is due to the dependence of the wall boundary-layer profile on Reynolds number. The relatively high number of the DC_{60} for low as well as large mass flows results from flow separation at the inner part of the lip. This is shown by the measured pressure distribution around the lip.

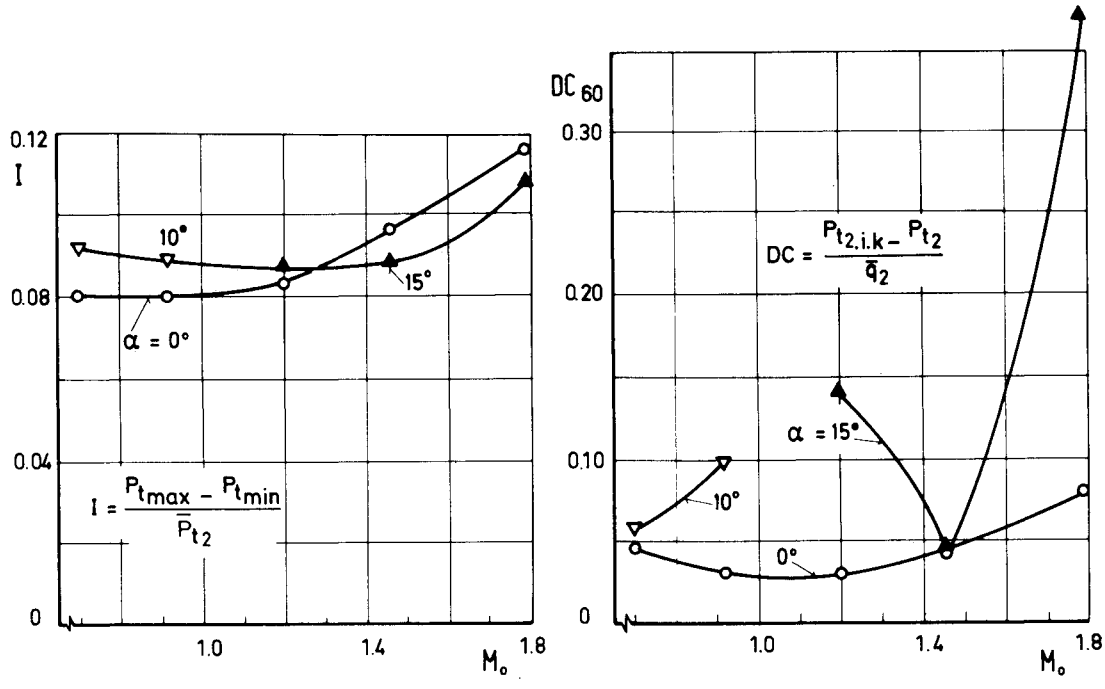

Fig. 10 Distortion indices I and DC_{60} vs Mach number, $M_1 = 0.75$.

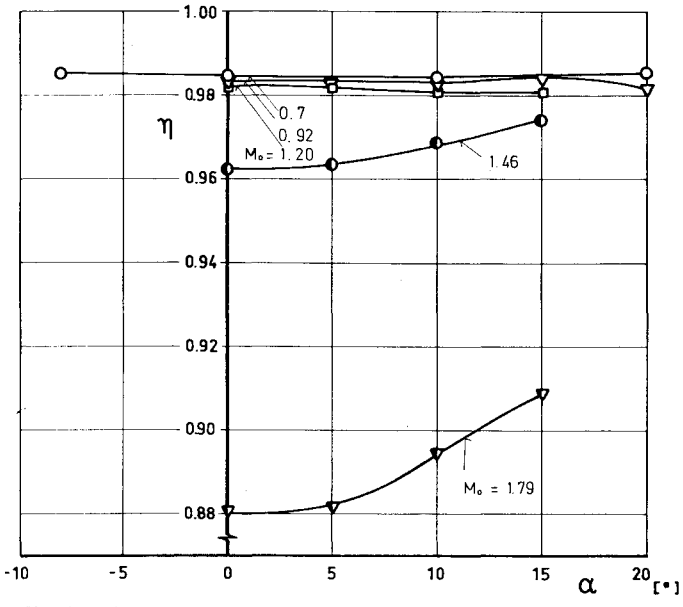

Fig. 11 Total pressure recovery, effect of angle of attack and Mach number, $M_1 = 0.75$.

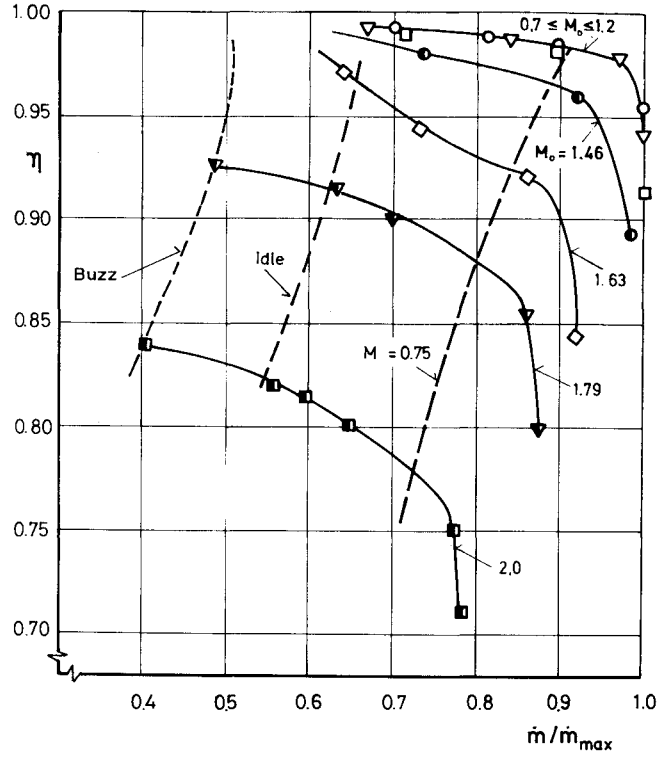

Fig. 12 Total pressure recovery, effect of mass flow and Mach number.

Pressure Recovery and Distortion at High Speeds

Inlet performance in terms of total pressure recovery and flow distortion indices is summarized in Figs. 9-12. Pressure recovery as a function of Mach number for $\alpha = 0$ and 10 deg is shown in Fig. 9. This figure shows that the total pressure loss is below 2% for Mach numbers less than 1.2. These losses are primarily due to friction along the inlet duct wall. For Mach numbers greater than 1.4 there is a rapid increase of the losses with increasing Mach number. Around this Mach number is the design point of the 11-deg ramp inlet. Up to $M_0 = 1.4$ the oncoming flow is decelerated by a detached shock. For higher Mach numbers, the inlet flow creates a normal shock in addition to the oblique one with subsequent higher losses. This situation is indicated in the figure by the dotted line and is discussed later in more detail. Finally, Fig. 9 shows the effect of angle of attack on the total pressure recovery. Locating the inlet in the protective flowfield of the forward fuselage significantly enhances the maneuver potential of an aircraft.

The distortion indices I and DC_{60} are plotted vs Mach number in Fig. 10 for $\alpha = 0$, 10, and 15 deg. It is seen that there are no dramatic changes of distortion with Mach number and of angle of attack, except at $\alpha = 15$ deg where $M_0 = 1.8$, which is an unrealistic flight condition. The airplane forebody is a powerful flow straightener significant in maintaining high inlet pressure recovery and low distortion at high angles of attack. Figure 11 shows total pressure recovery against angle of attack for different Mach numbers. The precompression for

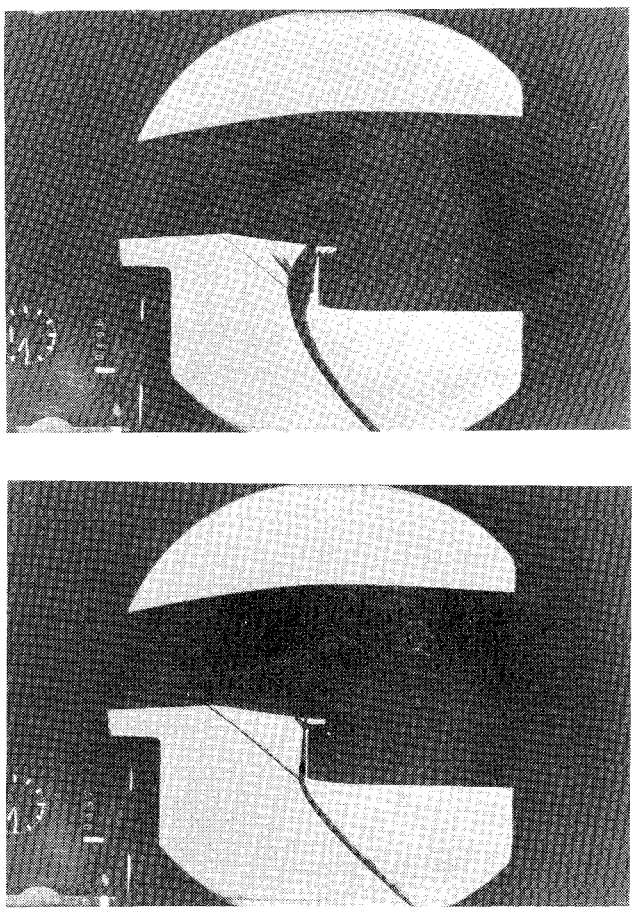

Fig. 13 Schlieren picture; demonstration of buzz, $M_0 = 1.79$.

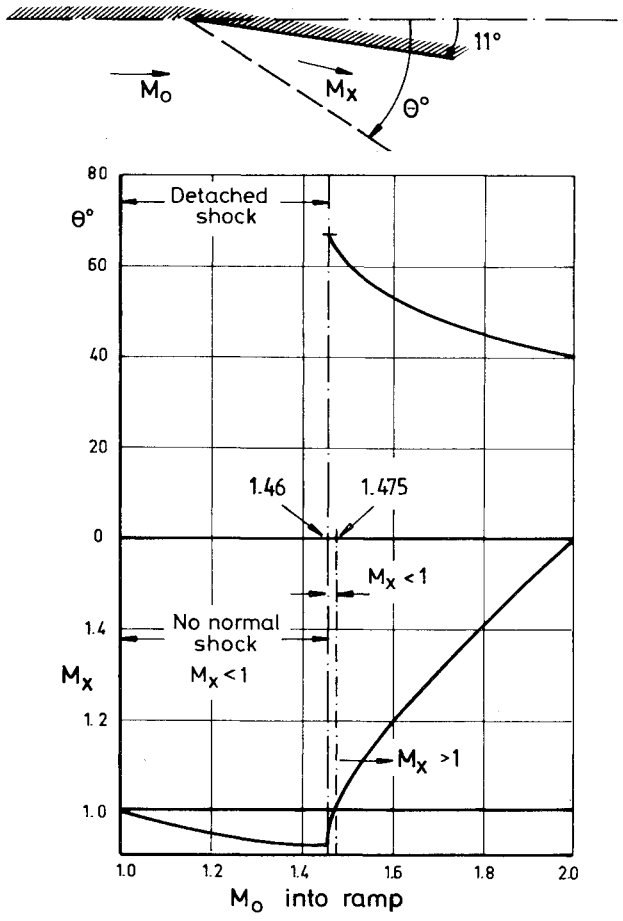

Fig. 14 Eleven-degree ramp, two-dimensional supersonic flow characteristics.

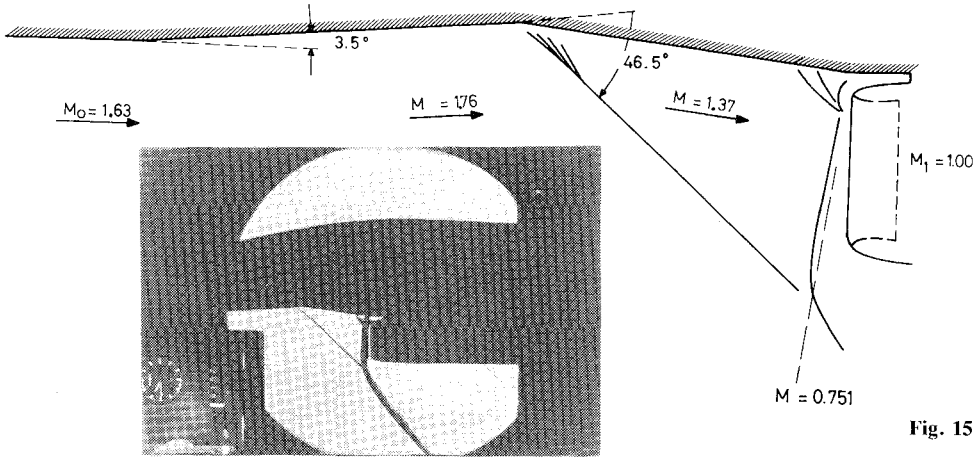

Fig. 15 Analysis of inlet flowfield, $M_0 = 1.63$.

the underfuselage location is significant for Mach numbers greater than 1.2. Figure 12 shows the effect of varying engine airflow at $\alpha = 0$ deg. Total pressure recovery increases with decreasing mass flow. The rapid reduction in total pressure recovery is indicative of choked flow at the throat of the inlet. The dotted line on the right-hand side indicates the mass flow equal to a throat Mach number of 0.75, which is close to the maximum airflow condition of a typical engine. The dotted line on the left-hand side indicates the mass flow for the idle condition of an engine similar to the F100-PW-100, see Ref. 1, Fig. 15.

Low Airflow Stability

During the high-speed tests the inlet was throttled to the "buzz" limit. "Buzz" was measured by means of a high-frequency sensor installed in the wall in front of the engine face. "Buzz" was indicated by a sudden increase of the turbulence signal of the sensor. Figure 12 shows the buzz limit as a function of mass flow and Mach number. Flow instability was found for $M \geq 1.46$ and occurs for flow conditions for which the intersection of the oblique and normal shock (triple point) is within the capture area. The schlieren picture, Fig. 13, demonstrates this very well. Presumably a strong

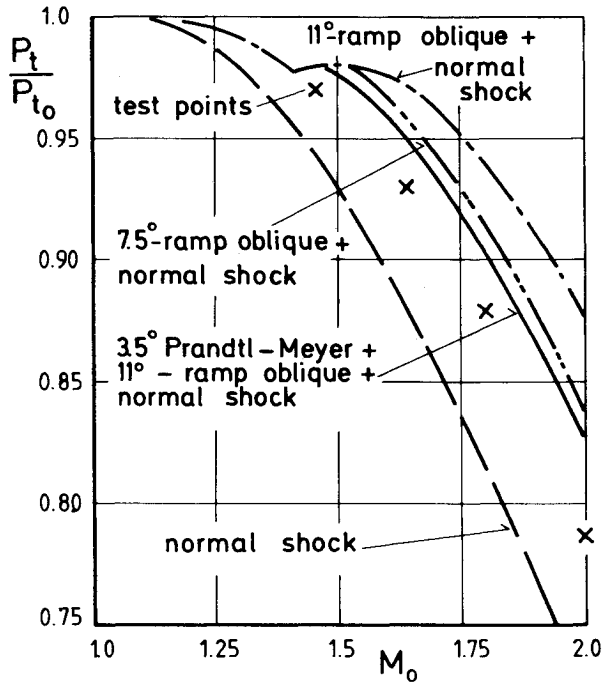

Fig. 16 Total pressure recovery vs Mach number; comparison of different configurations with EM-1 tests.

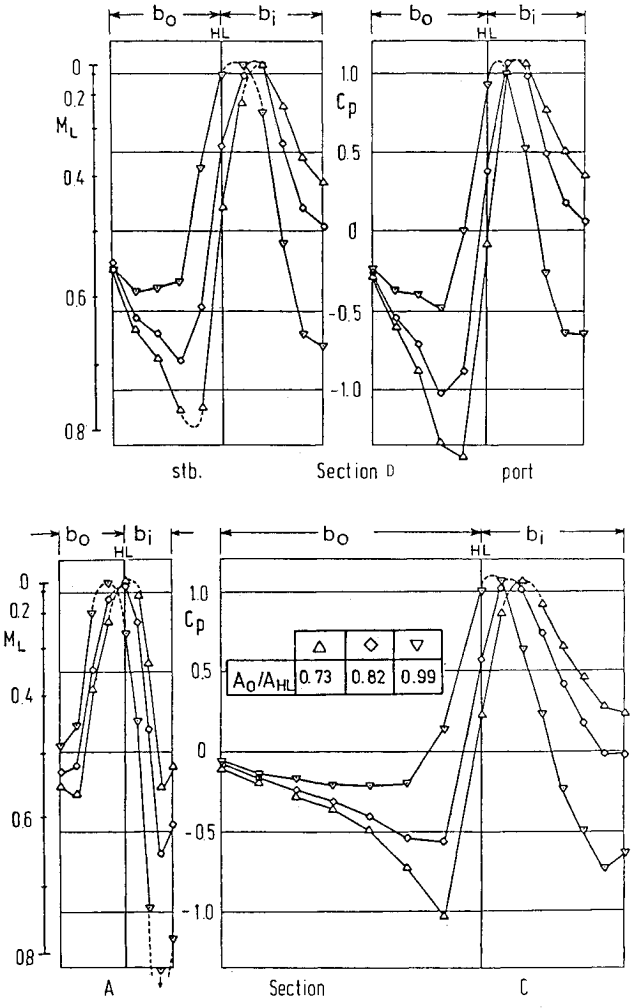

Fig. 17 Lip pressure distribution plotted perpendicular to freestream direction, $M_0 = 0.5$, $\alpha = 0$ deg; effect of capture area ratio.

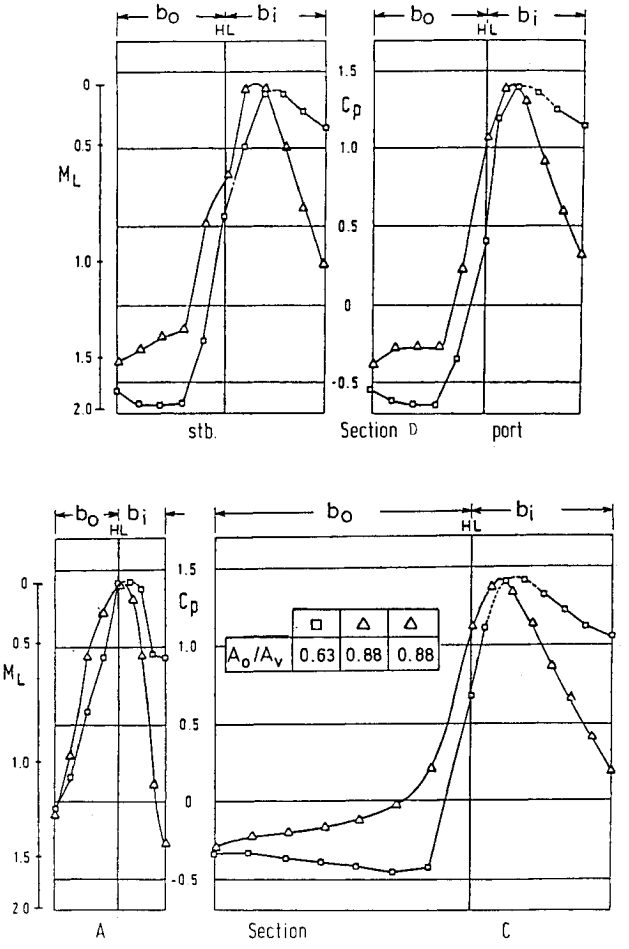

Fig. 18 Lip pressure distribution plotted perpendicular to freestream direction, $M = 1.2$, $\alpha = 0$ deg; effect of capture area ratio.

shock/boundary-layer interaction, not seen in the figure, causes a thick boundary layer that may flow into the inlet. For this reason, a forward-extended, thinner upper lip, such as on the F-16 inlet may be beneficial in reducing buzz airflow.

Analysis of the Supersonic Inlet Flow

The wave angle and the Mach number downstream of the shock wave as a function of freestream Mach number for two-dimensional supersonic flow with an 11-deg deflection angle are shown in Fig. 14. There are three different flow systems depending on the freestream Mach number M_0. From $M_0 = 1$ to 1.46, the shock is detached and the Mach number behind the shock is subsonic. For $1.46 < M_0 < 1.475$, the oblique shock is attached but the Mach number behind the shock is subsonic. For $M_0 \geq 1.475$, the Mach number behind the shock is supersonic.

Figure 15 shows a schlieren picture of the inlet flow for $M_0 = 1.63$. The oblique shock is attached and the 46.5 deg wave angle corresponds to a Mach number of 1.76 in front of the shock and 1.37 behind the shock. The flow acceleration from $M_0 = 1.63$ to 1.76 in front of the shock comes from the expansion along the conical forebody. A normal shock in front of the inlet causes the flow to decelerate from $M = 1.30$ to 0.751 with a further acceleration to sonic Mach number for the choked throat condition. The schlieren picture shows a local shock system ahead of the upper lip; due to the blunt lip, a detached shock and local separation are expected. It is recommended for a new design to make the upper lip thinner.

A similar investigation of the flowfield was performed for Mach numbers of 1.2 and 2.0. It was found that the best fit between the experiment and supersonic two-dimensional flow theory was obtained by assuming a 3.5-deg Prandtl-Meyer ex-

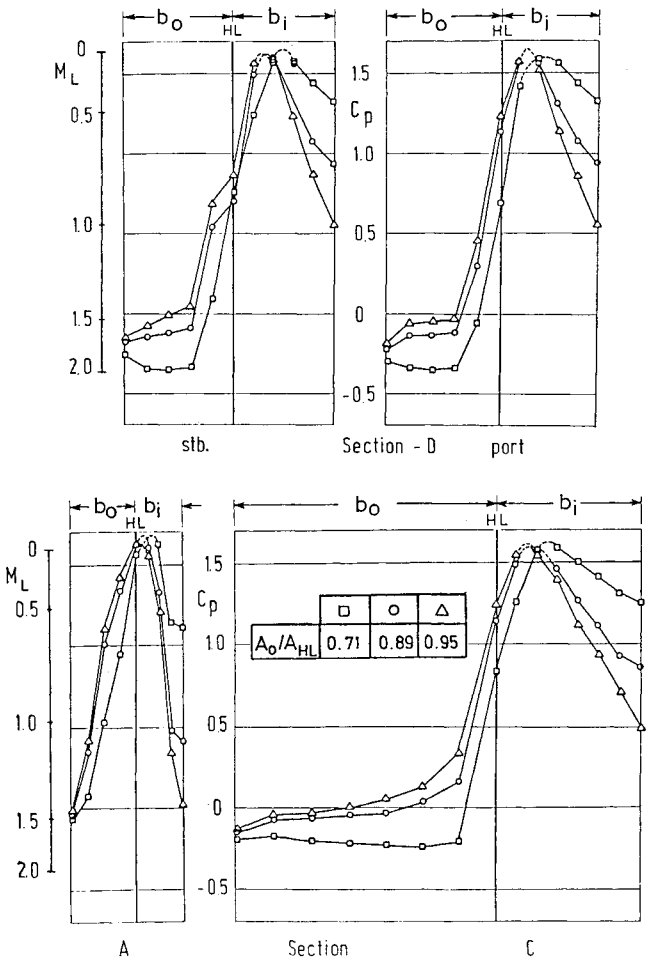

Fig. 19 Lip pressure distribution plotted perpendicular to freestream direction, $M = 1.46$, $\alpha = 0$ deg; effect of capture area ratio.

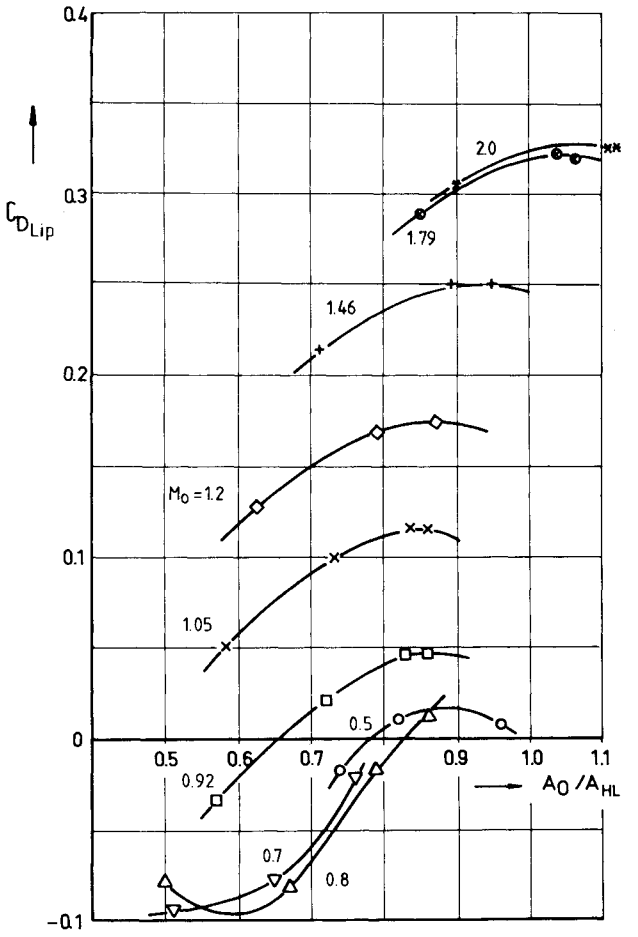

Fig. 20 Axial force on lip vs capture area ratio and freestream Mach number.

pansion on the forebody, an 11-deg ramp oblique shock compression, and a final normal shock compression to subsonic Mach number in front of the inlet. Figure 16 shows the total pressure behind the final shock vs Mach number calculated for the four different flow models: 1) normal shock, 2) 3.5-deg Prandtl-Meyer expansion plus 11-deg ramp oblique shock plus normal shock, 3) 7.5-deg ramp oblique shock plus normal shock, and 4) 11-deg range oblique shock plus normal shock. The measured total pressure recovery at the engine face is also shown in Fig. 16. The best agreement between experiment and theory is obtained with the second flow model. From the figure it is obvious that the expansion at the forebody results in large reduction in pressure recovery. To obtain full advantage of the 11-deg ramp, it is recommended that the lower surface of the forebody be as flat as possible.

Axial Force on the Inlet Lip

The drag of the lip was found by integrating more than 100 pressure measurements around the lip at seven sections of one-half of the inlet. Figure 17 shows the pressure distribution in terms of C_p plotted vs the thickness of the lip at four sections for $M_0 = 0.5$ and three capture ratios. On the outer lip contour the most downstream point has nearly freestream pressure. A suction peak is near the highlight but outside. The suction increases with decreasing mass flow. The stagnation points are near the highlight but inside the duct and the local Mach number inside the duct increases with increasing mass flow. The area under the pressure distribution curves gives a measure of the axial force acting on the lip. It is shown below that for a capture ratio of $A_0/A_1 = 1$ the axial force is zero and for $A_0/A_1 < 1$ the axial force is in the forward direction.

The pressure distribution around the lip for supersonic Mach numbers of 1.2 and 1.46 is shown in Figs. 18 and 19, respectively. Compared to Fig. 17, it is interesting to note that there is practically no suction peak at and outside the highlight point, and it is obvious that for all three capture ratios there is a high aft-directed axial force. This result corresponds well with theoretical calculations of the pressure distribution with a Euler method for the same inlet without the forebody.[3] Similar to an airfoil at supersonic speeds, the inlet lip has wave drag. This is shown in Fig. 20, where the axial force coefficient obtained by integrating the pressure distributions is plotted vs capture ratio for different Mach numbers.

For subsonic Mach numbers and capture area ratio $A_0/A_{HL} = 0.86$, which corresponds to a capture area ratio of 1 with the throat as the reference area, the axial force is approximately zero. For smaller mass flow ratios there is a forward-directed axial force, as expected. For the transonic and supersonic Mach numbers there is the same tendency of decreasing axial force with decreasing capture area ratio but the level of the rearward-directed axial force increases with increasing Mach number. The only means to reduce the wave drag of the lip is to make the lip thinner. At high supersonic Mach numbers, for some test points the capture area ratio is seen to be greater than 1. This is because A_{HL} is not the true inlet capture area.

Some measurements of the total pressure in front of the lip and normal to the ramp show that the momentum thickness of the boundary layer is in the range of 6-10 mm. This confirms the selection of 10 mm for the distance between the fuselage and the upper lip, see Fig. 2. Concerning the thickness of the rest of the lip, one has to make a compromise between the following: the thinner the lip the higher the subsonic total pressure losses, and the thicker the lip the higher the super-

sonic wave drag. Putting the thicker part of the lip inside the inlet will increase the capture area and is, therefore, not favorable. The influence of the lip thickness on the subsonic total pressure recovery is given in Ref. 4. Handbook methods using wave drag are not available, but more information will soon be available using Euler methods.

Conclusions

The fixed-geometry, pitot-type inlet design in an underbelly location with a fuselage-integrated 11-deg ramp and a boundary-layer splitter provides high pressure recovery and low flow distortion over a wider range of Mach numbers then the pure pitot-type inlet. The inlet airflow is stable for reduced mass flow up to a very high angles of attack. The relatively blunt leading edge of the inlet tip creates supersonic wave drag. The following recommendations are for such an inlet design.

1) Flow expansion on the forebody in front of the ramp should be avoided by flattening the forebody.

2) A ramp angle of 11 deg is near optimum for Mach numbers of 1.4-1.5, as shown in Fig. 16.

3) The leading edge of the upper lip should be sharp and extended forward by one-third of the ramp length.

Acknowledgments

This work was sponsored by the German Ministry of Defense.

The author wishes to thank Hartmut Buers, Dr. Donald Ritchie, Ernstfried Thiel, and Herbert Zimmer of Dornier GmbH Friedrichshafen, and Reinhard Friedrichs, Dr. P. A. Mackrodt, and Dr. E. Wedemeyer of DFVLR, Braunschweig and Göttingen, for their contributions to this paper.

References

[1]Hawkins, J.E., "YF-16 Inlet Design and Performance," AIAA Paper 74-1062, 1974.

[2]Leamar, P.C. and Kennon, I.G., "Experimental Investigation of a 0.15-Scale Model of an Underfuselage Normal-Shock Inlet," NASA CP 3049, 1978.

[3]Grashof, J. and Schmidt, W., "Computational Methods for Two-Dimensional and Three-Dimensional Inlets in Subsonic and Supersonic Flow," ICAS-82-4.3.1, 1982.

[4]Ball, W.H., "Propulsion System Installation Corrections," AFFDL-TR-72-147, Vol. 1, Dec. 1972.